International Journal of Automotive Technology, Vol. 20, No. 2, pp. 397–410 (2019)
DOI 10.1007/s12239–019–0039–2

pISSN 1229–9138/ eISSN 1976–3832

DRAG REDUCTION OF A PASSENGER CAR USING FLOW CONTROL TECHNIQUES

Akshoy Ranjan Paul[1)*], Anuj Jain[1)] and Firoz Alam[2)]

[1)]Department of Applied Mechanics, Motilal Nehru National Institute of Technology Allahabad, Prayagraj 211004, India
[2)]School of Aerospace, Mechanical and Manufacturing Engineering, RMIT University, Melbourne 3083, Australia

(Received 8 May 2017; Revised 4 March 2018; Accepted 19 October 2018)

ABSTRACT–The paper describes flow control techniques viz. vane-type vortex generator (VG) array and rear-spoiler on its trunk (boot) side used to reduce drag of a passenger car. The experimental and computational studies were carried out and different cases and combinations were analyzed for the car model by varying incoming airflow angle and spoiler angle and orientations of VG array to find out the optimum conditions for which drag coefficient is found minimum. Shear stress transport (SST) *k-w* turbulence model is found suitable in predicting the multi-scale rear-wake vortices of the car geometry. It is found that the crossflow increases the drag coefficient, which can however be reduced effectively if both VG array and rear-spoiler are used. Parametric analysis shows that counter-rotating VG array is found useful in reducing drag (around 23 %) as it promotes better flow mixing at its downstream, which is helpful in avoiding flow separation. The finding is also supported by the flow visualization study. It is also found that saving up to 11.5 % in the fuel consumption can be achieved by reducing drag using these techniques. The wake analysis and turbulent kinetic energy plots indicated that the counter-rotating VG array while used with a rear spoiler parallel to the flow reduced drag considerably.

KEY WORDS : Car aerodynamics, Flow separation, Vortex Generator (VG), Rear spoiler, Drag coefficient, Turbulent Kinetic Energy (TKE)

NOMENCLATURE

C_D : drag coefficient (dimensionless)
C_L : centerline length of car (mm)
C_p : wall static pressure coefficient (dimensionless)
C_μ : turbulence model constant
H : height of car model (mm)
k : turbulent kinetic energy (m^2s^{-2})
L : length of car model (mm)
l : length of rear spoiler (mm)
p : static pressure (Nm^{-2})
Re : reynolds number (dimensionless)
u : velocity (ms^{-1})
W : width of car model (mm)
x, y, z : coordinates

GREEK LETTERS

α : rear spoiler angle w.r.t. flow (degree)
β : car angle w.r.t. flow (degree)
ε : turbulent kinetic energy dissipation rate (m^2s^{-3})
ν : kinematic viscosity coefficient (m^2s^{-1})
ω : specific dissipation (s^{-1})

SUBSCRIPT

i : vector indices

1. INTRODUCTION

A highly complex and critical segment in the field of automotive development is the design of passenger car body. A number of constraints in the car body design such as space, aesthetics, attractiveness, style and aerodynamically-refined body makes it a challenging one. Researchers have so far been focused upon optimal design to reduce drag and consequently improve vehicle performance based on a simplified vehicle model known as 'Ahmed body' as proposed by Ahmed (1981). The wake region behind this bluff body to an extent dictates the drag. There have been various researches (Ahmed *et al*., 1984; Chan *et al*., 2008a, 2008b) on wake structures behind this model to understand the wake dynamics in order to reduce drag. Due to the over simplification of the Ahmed body model, more complex flow phenomena, e.g. at the underbody and the wheels/wheelhouses, cannot be reproduced. To overcome it, a new car model has been proposed by Heft *et al*. (2012) which is successfully used for aerodynamic optimization of production vehicles.

The reduction of drag coefficient (C_D), which is mostly influenced by the exterior profile (shape) of the car remains

**Corresponding author.* e-mail: arpaul@mnnit.ac.in

one of the major concerns in the field of the automotive research (Hucho, 1998) as it is also responsible for fuel economy. Average C_D values are reduced remarkably over the time, from 0.7 for old box-type cars to a mere 0.3 for the streamlined shaped modern ones (Katz, 1995). Song *et al*. (2012) proposed an aerodynamically optimized outer shape of a sedan by using an Artificial Neural Network (ANN), which focused on modifying the rear body shapes of the sedan. Using body shape optimization, a 5.6 % reduction in C_D is achieved than that of baseline design. Achieving the reduction in aerodynamic drag whilst meeting the variable cooling demand for passenger cars is generally limited by packaging and stylistic constraints as the drag coefficients have plateaued at around 0.28 since 2012 (Watkins and Alam, 2012).

For high speed passenger cars, the aerodynamic pressure drag is predominant due to the flow separation, particularly on the rear window and on the wheel base (Geropp and Odenthal, 2000). This contribution corresponds to 90 % of total aerodynamic drag and 80 % of this contribution is due to the rear part of the car (Kourta and Gilliéron, 2009).

One of the key sources of aerodynamic drag over passenger cars is the separation of flow near the vehicle's rear end. Large energy losses are often associated with boundary layer separation. A common flow separation control method is to add momentum to the near wall flow by redirecting the higher momentum from the free-stream or the outer region of the boundary layer into the separation zone.

Kang *et al*. (2012), on the other side, developed an actively translating rear diffuser device to reduce the aerodynamic drag experienced in passenger cars and achieved over 4 % reduction in drag coefficient.

Recently, Cho *et al*. (2017) investigated the effects of the interactions based on the combination of the aerodynamic drag reduction devices-like an undercover, under-fin, and side air dam on a sedan-type car. It was found that the undercover reduced the slipstream area through the attenuation of the longitudinal vortex pair by enhancing the up-wash of underflow, thereby reducing the aerodynamic drag of the car by 8.4 %.

There are two major influences on the distribution of surface pressures on bluff-bodies especially automobiles. One is simply the size of the apparent surface in flow direction and the other is the interaction of flow features with the body. A rise of localized surface (by adding a spoiler or VG) will induce bigger surface pressures on this area and change global surface pressures. Furthermore, a change in upstream flow features (in crosswind conditions) can also have an influence in the surface pressure distribution on the body. Hence, there are two ways of varying local surface pressures on a vehicle: by geometrical and/or aerodynamic variation.

In the automobile domain, there has been an increasing interest in the link between safety and stability in crosswind interaction. Vehicles under strong cross-flow become vulnerable due to stability issue (Gillhaus and Hoffmann, 1998). The stability of the vehicle may be increased by increasing the traction between the tyres of the vehicle and the road surface. Moreover, road vehicles can experience wind from any direction. Hence the fuel economy of passenger cars is generally estimated based wind averaged drag. Hence, it is utmost important to quantify the effects of crosswind on drag.

Two factors that have major influence on the drag coefficient of a bluff object are the roundness of its front corners and the degree of taper at its rear end (Schlichting and Gersten, 2007). The importance of the influence of the rear taper in passenger cars can be described as 'spoiler' on rear car body. Such spoilers are often fitted to passenger cars at the trunk rear. The main design goal of a 'rear spoiler' in passenger vehicles is to increase traction and better grip on the road surface (Katz, 2006). Rear spoiler modifying the shape transition between the roof and the rear, and the trunk and the rear does act in minimizing the turbulence at the rear of the vehicle. Adding a rear spoiler makes the air 'travel' a longer and gentler slope from the roof to the spoiler delaying the flow separation. But this does not imply that spoiler decreases drag, the sole purpose of a spoiler is to improve the traction and in this process, the drag may be increased. However, if used of certain design and at certain orientation, the spoiler can also reduce drag, but that would consequently results in reduction of traction.

Rouméas *et al*. (2008) reported that a local suction system located on the upper part of the rear window is capable of eliminating the rear window separation on simplified fastback car geometry and C_D can be reduced by 17 %. Hassan *et al*. (2014) computationally achieved 22.13 % drag reduction using rear under body modification. Cakir (2012) achieved around 17 % drag reduction with a modified rear spoiler for a sedan car. Recently, Cheng and Mansor (2017) also discussed the effect of rear-spoiler angle on aerodynamic drag of a simplified hatchback car model. These studies motivated the authors to carry out an extensive experimental and computational study to investigate the combined effects of rear-spoiler and VG array on a sedan car model.

The main purpose of this paper is to develop an effective method of flow control at the car downstream in order to reduce drag and impart stability. The present investigation is focused on flow control by vortex generators (VG) in combination with the rear spoiler. The overall effect of the VG array and the rear spoiler depend on the variation of the shape and size of VG and the spoiler angle.

Experimental investigation was carried out to optimize aerodynamic drag and surface static pressure using a geometrically similar, 15:1 reduced scale model of a Sedan type 'Honda City' car as shown in Figure 1, differing from actual car only in size and simulating dynamically similar flow situations in a blow-down type subsonic wind tunnel. This included flow visualization techniques (viz. oil-flow

and smoke flow), which were used to establish the effectiveness of the VG and rear spoiler, and their best combination at which the drag coefficient was minimum.

2. EXPERIMENTATION

The experiment was performed in an open-circuit, blow-down type subsonic wind tunnel. The test-section was made with transparent Perspex sheet for visual observation of the car model. It has an outer cross-section of 500 mm × 500 mm with a length of 2500 mm.

2.1. Test Model

The test model of a car is geometrically similar to the prototype (Honda City) with reduced scale of 15:1 having following dimensions: car model length (L) is 300 mm along x-axis, width (W) is 110 mm along z-axis, and the height (H) is 100 mm along the y-axis. The ground clearance between the car underbody and the tunnel floor is kept as 11 mm and is shown in Figure 1. The blockage ratio (i.e. the frontal projected area of the car to the wind tunnel test-section area) for the present wind tunnel study is 4.4 %, which is reasonable.

2.2. Boundary Layer Study

Boundary layer growth over the car at free-stream velocity of 36 m/s while facing the flow at 0° incidence angle is very small and the boundary layer thickness is measured as 2 mm at the upstream, and it is increased to 3.5 mm at the midstream of the car (Figure 2). The vortex generators have been designed based on the boundary layer thickness and are placed along the car width at x/L = 0.703, which

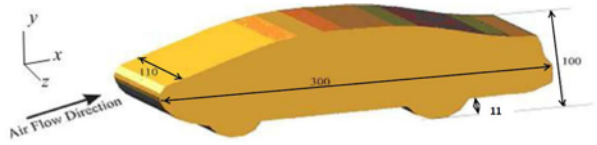

Figure 1. Geometry of the car model.

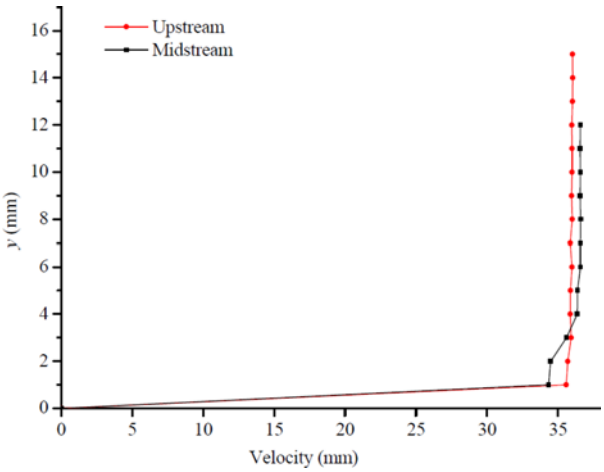

Figure 2. Boundary layer growth over the car.

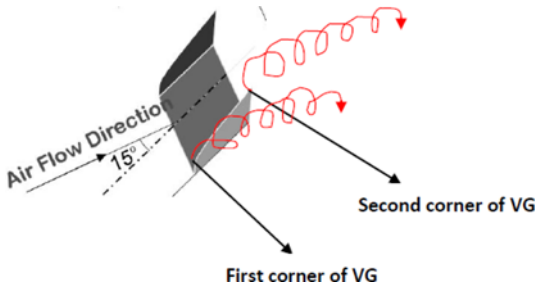

Figure 3. Corner vortices shedding from trapezoidal VG.

corresponds to the line where the car roof ends, beyond which the flow is likely to get separated as evident from the literature. Since the flow control technique (e.g. VGs) is to be employed on or before the onset of flow separation, this location of VG is chosen. The maximum height of the vortex generator is kept as 2 mm, and hence the VG array is completely submerged to the boundary layer thickness. Hence, this type of VG is occasionally called 'submerged trapezoidal VG'.

2.3. Vortex Generators

The advantage of trapezoidal vortex generator (VG) is that it has two corners having different elevation with respect to the flow direction, which create vortices simultaneously (Lin, 2002). The vortices created by the first corner is convected to the downstream uninterruptedly even after the additional vortices are created by the second corner due to

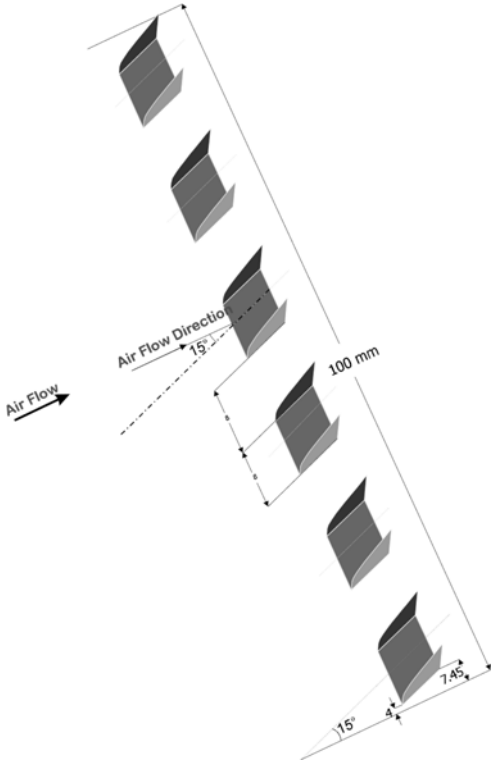

Figure 4. Schematic of co-rotating VG array.

change in elevation, thus provides an effective means of suppressing massive flow separation caused in the downstream as shown in Figure 3.

Therefore, such VG while arranged in an array protrude into the air flow and induces local flow separation, causing a tight swirling pattern to develop in the flow. This increased momentum can help keeping airflow attached over sharp direction changes. This effect can reduce flow separation at areas like the rear windshield of a car and reduce the low pressure area developed there. Two types of VG were used in this study: co-rotating and counter rotating. Co-rotating VG is trapezoidal shaped vertical plates placed in parallel to each other as shown in Figure 4.

In the counter-rotating VG, trapezoidal shaped vertical plates are placed at an angle of 30° to each other (Figure 5). In co-rotating type VG, vortices are produced in clockwise direction, while counter rotating VG generates vortices in counter-clockwise direction.

The advantage of trapezoidal VG is that it has two corners having different elevation with respect to the flow direction, which create vortices simultaneously (Lin, 2002). The vortices created by the first corner is convected to the downstream uninterruptedly even after the additional vortices are created by the second corner due to change in elevation, thus provides an effective means of suppressing massive flow separation caused in the downstream.

2.4. Rear Spoiler

A spoiler is simply a device that slows and collects air, causing it to stagnate. The most common spoilers are placed at the rear end of the car, over the trunk (boot). The rear spoiler creates an area of relatively higher pressure to replace the usual low pressure over the trunk (boot).

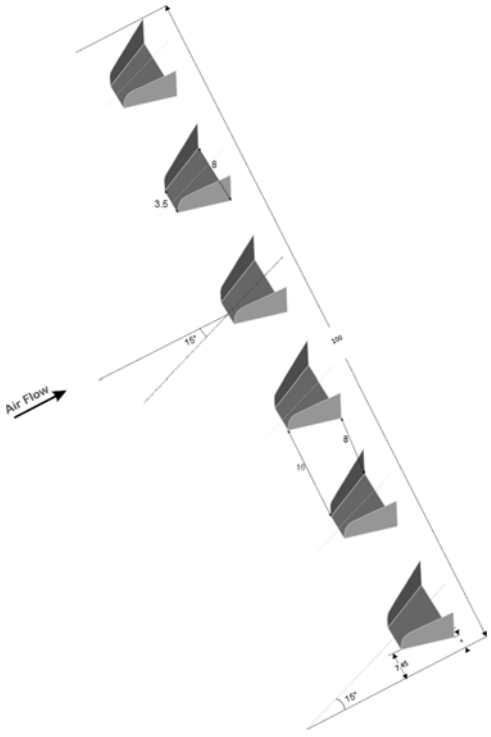

Figure 5. Schematic of counter-rotating VG array.

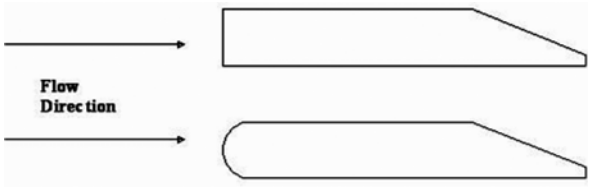

Figure 6. Side view of rear spoiler (rectangular and semi-circular).

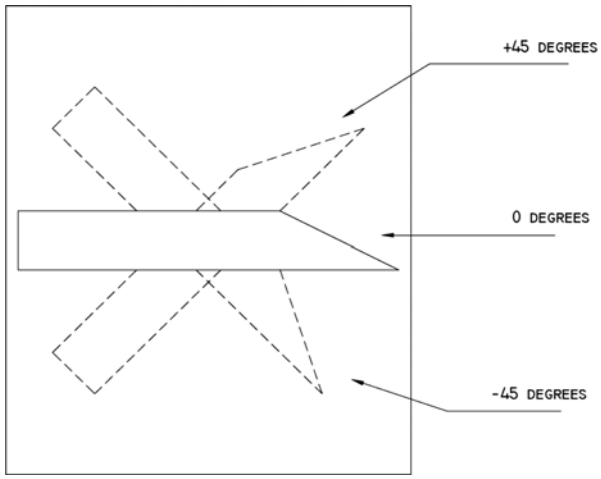

Figure 7. Orientation of rear spoiler.

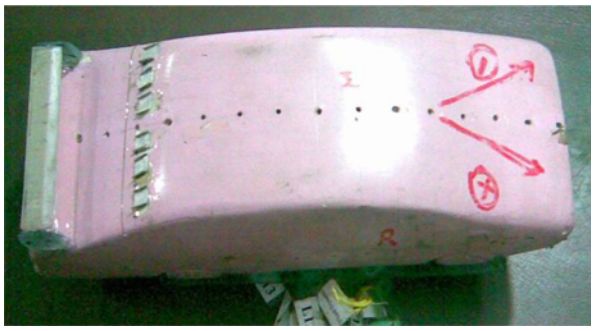

Figure 8. Locations of pressure holes, co-rotating VG array and rear spoiler on the car.

The length of the rear spoiler attached to the car model is 98.5 mm, width 16 mm and thickness 5 mm. The height of the spoiler-support is 19.8 mm and its thickness is 1.6 mm. Two side-sections of the spoiler are used in the study: rectangular and semi-circular as shown in Figure 6. The spoiler angle (a) varies from + 45° (above the flow direction) to − 45 (down the flow direction) as shown in Figure 7. The locations of pressure holes, co-rotating VG array and rear spoiler on the car are shown in Figure 8. Seventeen pressure holes are provided each on the mid-line of the roof and both sidewalls of the car.

Table 1. Least count and uncertainty measured.

Parameter	Instrument	Least count	Uncertainty
Vertical traverse	Probe traversing mechanism	0.1 mm	± 0.1 mm
Pressure	Digital micro-manometer	0.001 N/m^2	± 0.025 % of FSD
Ambient temperature	Digital thermometer	0.5 °C	± 0.5 °C

2.5. Instrumentation

A series of measuring equipment is used for the flow study. Telescopic Pitot-static tube: It is a pressure measuring instrument used to monitor flow velocity at the upstream of the car model.

Calibrated five-hole pressure probe with transverse mechanism: It is used to measure the three components of velocity, inflow angles (pitch and yaw), static and total pressures simultaneously for a point in a flow field. The probe is positioned using rack and pinion based traversing mechanism and the pressure is measured with the digital micro-manometer connected to it via a digital pressure scanner.

Digital micro-manometer coupled with pressure scanner: It allows the pressure signal delivered to an instrument to be scanned or switched between multiple pressure sensors.

Digital vane anemometer: This instrument provides fast, accurate readings with digital readability and the convenience of a remote probe. The metal vane anemometer is used to measure the flow velocity at the exit of the test-section.

The least count and uncertainty are furnished in Table 1.

2.6. Flow Visualization

It is important to visualize the streamlines on the surface of the car for better understanding of separation and reattachment of flow. For this purpose, oil-flow visualization technique is one of the best methods available. This gives a brief idea about the pattern of flow on the surface of the car model. The problem arises in selection of chemicals and making a mixture which gives clarity, showing streamlines clearly. For oil-flow visualization in the present study, three materials were used: titanium dioxide, oleic acid and kerosene oil. All the materials had some specific properties which played important role in flow visualization.

Titanium dioxide is a white powdery pigment as the surface of the car was made black (Figure 14), this would give a better contrast producing clear pattern of flow, and moreover it is a non-toxic pigment. Oleic acid was used as an additive to titanium dioxide to increase the boldness of the streamlines. Kerosene oil was used for the purpose of utilizing its volatility and it allows the pattern to develop in the prevailing condition of air flow and later would completely vaporize leaving behind a clear pattern of flow. The oil mixture contained 5 ml water, 4 to 5 gm titanium dioxide powder, 2 ml oleic acid, 4 ml kerosene oil. The color of the mixture was white. The mixture was painted over the desired location of the car using a spray gun prior to flow visualization. Then the experiment was carried out in a low-speed wind tunnel at a free-stream velocity of 30 m/s for 10 minutes. The air flowed over the car, and left hairline pattern (in black and white combination) on the painted surface. The painted surface was then photographed using a digital camera under proper illumination. The digital photograph was then analyzed using an image processing toolbox facility provided in MatLab^{TM} software. The color intensity variation is plotted along the predefined locations.

Similarly, for smoke visualization, non-toxic white smoke was released from the smoke generator and the visualization was conducted at low velocity (10 m/s) to see the flow pattern over the rear spoiler.

3. COMPUTATION

For drawing the car geometry, commercial CAD software was used. ICEM-CFD was used for three-dimensional grid generation. The flow simulation is carried out in a commercial CFD solver Ansys-Fluent on a IBM Workstation.

3.1. Computational Domain

The computational domain has dimension of 2500 mm along the *x*-axis, 500 mm along the *y*-axis and 500 mm along the *z*-axis. The car was placed 800 mm from inlet in the upstream and 1250 mm from the outlet in the downstream.

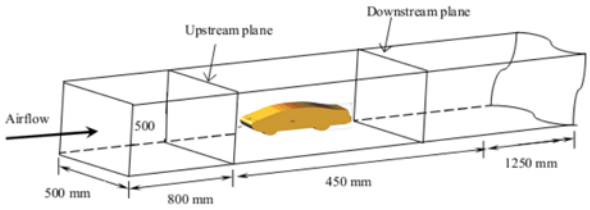

Figure 9. Computational domain of the car model for CFD study.

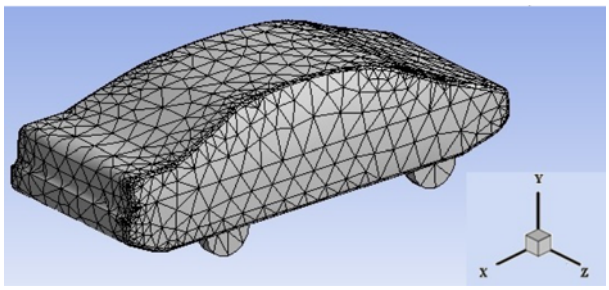

Figure 10. Meshing of car geometry (with rear spoiler).

Table 2. Grid independency test.

Sl no.	Number of cells	C_D
1	290526	0.3276
2	421901	0.3723
3	512080	0.3804
4	624828	0.3810

The first computing plane was taken 25 mm ahead of the car model in upstream direction and the second such plane was taken 125 mm from rear of the car where velocity and pressure contours were drawn. All the dimensions are shown in Figure 9.

3.2. Mesh Generation

Symmetry plane was considered along the longitudinal (*x*-*y*) plane, which bifurcated the car model as well the whole computational domain into two equal halves in order to reduce the computational effort. Tetrahedral (T-grid) meshing was used in this study as shown in Figure 10. T-grid meshing was preferred as the car geometry has irregular shape and is complex in nature. During the grid generation with and without VG array and rear spoiler, number of computational cells varied from 290526 to 624828. The grid independency test was performed and is tabulated in Table 2.

3.3. Mathematical Formulation and Numerical Techniques

For incompressible flow, the Reynolds Averaged Navier-Stokes (RANS) equations along with continuity equation are written as

Continuity equation:

$$\frac{\partial \overline{u}_i}{\partial x_i} = 0 \tag{1}$$

Momentum equation:

$$\frac{\mathrm{D}\overline{u}_i}{\mathrm{D}t} = -\frac{\partial\left(\overline{p} + \frac{2k}{\varepsilon}\right)}{\partial x_j} + \frac{\partial}{\partial x_i}\left[\nu_t\left(\frac{\partial \overline{u}_i}{\partial x_j} + \frac{\partial \overline{u}_j}{\partial x_i}\right)\right] \tag{2}$$

where turbulent viscosity ν_t can be empirically expressed as

$$\nu_t = C_\mu \frac{k^2}{\varepsilon} \tag{3}$$

3.4. Boundary Conditions

For the CFD simulation of the car model, the inlet velocity profile was taken same as experimentally obtained by Sagar (2010) for the bare car (i.e., car without any VG or spoiler), which was broadly uniform. Zero gauge pressure was specified at the exit for all simulation cases to compare the aerodynamic performance of the car. The car surface was treated as wall and no-slip boundary condition is specified at the side walls of the computational domain. Reynolds number (Re) is taken as 6.15×10^5 based on length of the car model (300 mm) and free-stream velocity of 30 m/s.

3.5. Discretization and Numerical Techniques

The steady, incompressible Reynolds Averaged Navier-Stokes (RANS) equations with second-order upwind discretization scheme were solved in the present study. Semi-Implicit Method for Pressure Linked Equations (SIMPLE) algorithm was chosen for computing velocity and pressures using pressure-based segregated Ansys-Fluent solver at different computational nodes. Suitable under-relaxation factors are set for pressure, momentum and turbulent kinetic energy in the solver. Convergence criteria was set at 10^{-5}.

3.6. Turbulence Model

With a wake structure of varying range of turbulence length scales, it is obvious that use of direct numerical solution (DNS) approach could fetch the best results but the objective and number of cases involved in the present study would not permit such methods as time requirement for DNS is extremely high. Hence Reynolds averaged Navier-Stokes (RANS) based turbulence model (Hanjalić, 1994) was used for it. Guilmineau (2008) shows that changing rear window slant angle from 25° to 35° entirely changes the turbulence model requirement. With such example, it is obviously difficult to predict a suitable turbulence model. Hence using all logically possible RANS models, analysis was made and the values of surface pressure and C_D for all models are compared with the experimental data to find the most accurate turbulence model for the present study.

The method employed for calculating drag in this study is based on Desai *et al*. (2008). The technique used to compute the C_D in numerical analysis allows the direct comparison of it with the measured C_D which is the sum of pressure drag and skin-friction drag. Table 3 gives the percentage errors for each turbulence model on full scale experimental data (namely surface pressure coefficient, C_p

Table 3. Percentage errors using turbulence models.

Turbulence model	Deviation in $C_p^{\dagger}$ (%)	Deviation in $C_D^{\ddagger}$ (%)
Standard k–ε	18.96	12.61
RNG k–ε	14.72	13.42
Realizable k–ε	9.65	8.89
Standard k–ω	24.12	16.68
SST k–ω	5.99	5.75

†with reference to experimental data (C_p at $\beta = 0°$), ‡with reference to experimental data (C_D at $\beta = 0°$) furnished in Table 4.

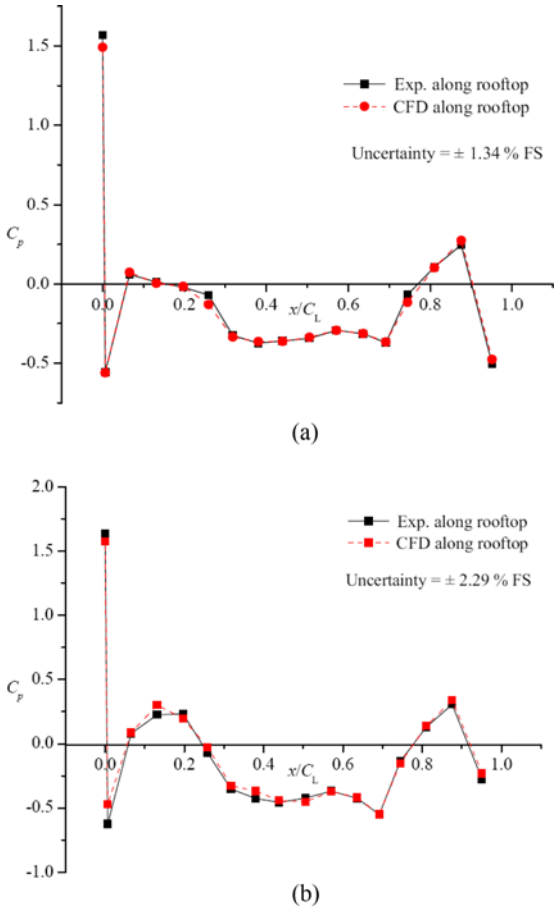

Figure 11. (a) C_p along the roof of car ($\beta = 0°$) with rear spoiler ($\alpha = -45°$) and co-rotating VG; (b) C_p along the roof of car ($\beta = 0°$) with rear spoiler ($\alpha = +45°$) and counter-rotating VG.

and drag coefficient, C_D). The table clearly shows that SST *k-w* turbulence model as proposed by Menter (1994) proves to be the most suitable for the car model (geometry). This is because the model uses different near-wall and away-wall techniques when both near-wall and away-wall flow are of significance. Enhanced wall treatment function was used in the present study.

3.7. Validation of CFD Code

The validation of the computational results based on a finite volume method (FVM) based CFD solver Ansys-Fluent is carried out with the experimental results of a Sedan type (model: Honda City) passenger car model. The computational results are matched with the experimental ones in terms of wall static pressure coefficient (C_p) on the car surface and drag coefficient (C_D). Wall static pressure is calculated at the 17 stations along the roof of the car. A sample of validation is presented in Figures 11 (a) and (b), where both rear spoiler and vortex generators are used on the car at different angles and orientations. The static pressure coefficient (C_p) graph confirms that the difference of computational and experimental readings of C_p falls within a narrow range.

The pressures at upstream and downstream planes (as shown in Figure 9) of the car model are measured using a five-hole probe. The difference of the pressure multiplied by the frontal area of the car gives the drag force and hence the drag coefficient (C_D). In case of CFD analysis, the same method was adopted to compute the C_D. Table 4 shows validation of C_D at different crossflow conditions.

4. RESULTS AND DISCUSSION

The experimental and computational analyses of drag reduction on a passenger car with vortex generator array and rear spoiler are presented in this section. The experimental analysis includes flow visualization using smoke and oil. The experimental data is also used to validate the CFD modeled data in this study.

4.1. Results of Bare Car

Bare car is defined as the car that does not have any flow control devices attached to it, i.e., car without spoiler and vortex generators (VG).

Car facing the wind is straightway ($\beta = 0°$), cross-wind from left side ($\beta = -30°$, left turn to the car) and from right side ($\beta = +30°$, right turn to the car) and the corresponding variations of wall static pressure coefficient (C_p) measured experimentally along the roof of the car is shown in Figure 12. In this figure, the variation of C_p along the roof of the car is negative which shows negative static pressure along the roof of the car indicating flow separation zone. It also shows C_p variation for $\beta = 0°$ depicting a rise in static pressure towards the end clearly indicates reattachment of flow. However, the cross-flow to the car increases flow separation, and further deteriorates the flow pattern. As a result, C_p values become more negative for cross flow condition.

Drag coefficient (C_D) is computed for the bare car and is compared to experimental data shown in Table 4. The error between experimental and computational C_D values varies

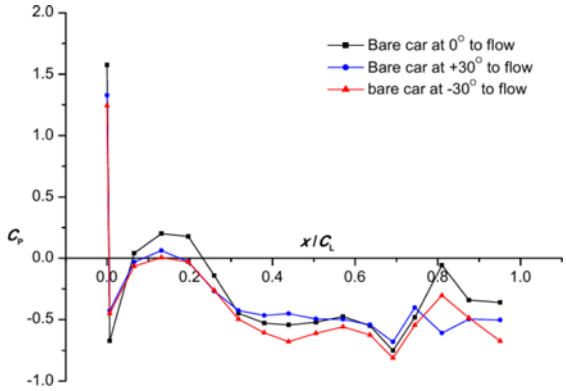

Figure 12. Effects of cross-flow on C_P distribution along roof of the car (experimental).

Table 4. Effects of cross-flow on C_D of bare car.

Car configuration	C_D (Exp.)	C_D (Comp.)
Car facing the wind (β = 0°) (i.e. no turn)	0.3597	0.3804
Car in cross-wind (β = + 30°) (i.e. left turn)	0.4991	0.5510
Car in cross-wind (β = – 30°) (i.e. right turn)	0.4858	0.5570

between 5 % and 14 %, which is considered to be acceptable range. This difference may be attributed due to considering the symmetry and using half of the car domain. When car is facing straightway to flow, C_D is low, whereas, C_D for the bare car facing crosswind is higher. This is due to the shape of the vehicle which is more aerodynamic while facing wind from the front as compared to while turning the car sideways with respect to the wind direction. Moreover, the projected area also increases when the car is turned sideways. This combined effect of shape and effective frontal area increase the net side force and creates larger flow separated areas causing instability and reduces safety of the car.

It is observed from Table 4 that the crossflow increases drag, and hence C_D. The judicious use of VG array can reduce the drag, while rear spoiler will impart the stability by increasing the traction.

4.2. Results of Car with Rear Spoiler

The side-sectional shape of rear spoiler attached to the car was varied as shown in Figure 6. However, the results show that a change from rectangular to semi-circular side-sectional shape of rear spoiler offers a negligible reduction (~ 0.36 %) in C_D. Therefore, the rest of the study was performed with a rectangular side-sectioned rear spoiler. Two extreme values (+ 45° or – 45°) of spoiler angle were considered for the study with respect to the reference value (0°) so that any intermediate value falls within the extreme limit.

4.3. Results of Car with VG Array and Rear Spoiler

The most common spoilers are placed at the rear end of the car, over the trunk. The rear spoiler creates an area of relatively higher pressure to replace the usual low pressure over the trunk (boot). Vortex generators (VG) are structures that protrude into the air flow and induce local flow separation, causing a tight swirling pattern to develop in the flow. This increased momentum can help keeping airflow attached over sharp direction changes. This effect can reduce flow separation at areas like the rear windshield and reduce the low-pressure area developed thereafter. The combined effects of the rear spoiler and VGs on C_p while the car facing the straight wind (β = 0°) are shown in Figure 13, whereas the C_D values found for selected combinations is listed in Table 5. It is noted that all combinations help in static pressure rise and drag reduction, however the maximum drag reduction (10.33 %) is reported for the car with rear spoiler at α = – 45° and co-rotating VG.

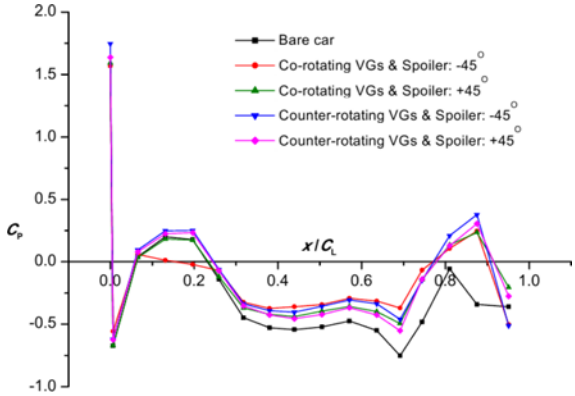

Figure 13. Effects of rear spoiler and VG on C_P distribution along roof of the car (experimental).

Table 5. Drag coefficient (C_D) of a few selected spoiler and VG array configurations for car at β = 0°.

Car configuration		C_D (comp.)	C_D Reduction
VG	Spoiler		
No	No	0.3804	Ref. value
counter-rotating	No	0.2939	22.73 %
co-rotating	No	0.2942	22.66 %
counter-rotating	α = 0°	0.3050	19.82 %
co-rotating	α = 0°	0.3052	19.76 %
counter-rotating	α = + 45°	0.3499	8.02 %
co-rotating	α = + 45°	0.3474	8.68 %
counter-rotating	α = – 45°	0.3532	7.15 %
co-rotating	α = – 45°	0.3411	10.33 %

It is observed from Table 5 that counter-rotating VG array has slight edge over co-rotating one in order to reduce drag of a car. This is probably due to the fact that the counter-rotating VG array produces vortices, which has a high tendency to mingle with adjacent vortices, and thereby assists in momentum transfer from lower momentum to higher momentum fluid layer.

As a result, the flow separation can be controlled effectively using counter-rotating VG array. The fact is supported by the flow visualization results described in the following section.

4.4. Flow Visualization

For all cases, a particular area over the rear end of the car (x/C_L = 0.54 to 1.0) was selected for oil flow visualization as shown in Figure 14 and marked as a yellow block. For

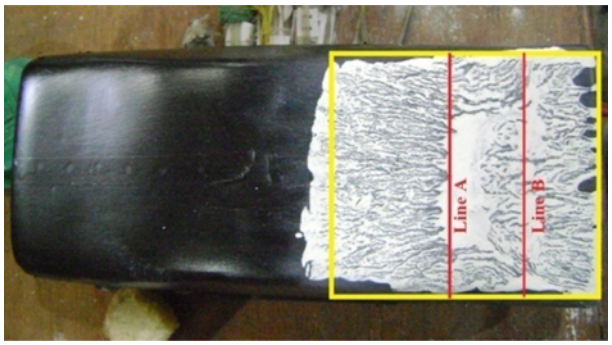

Figure 14. Top view of bare car with oil flow visualization at the rear.

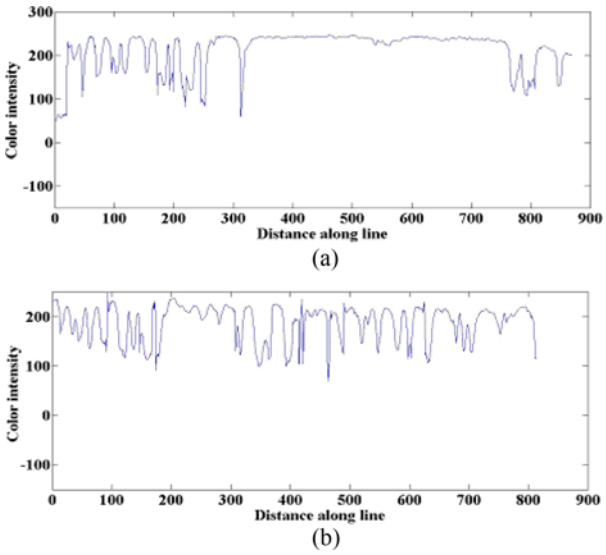

Figure 15 (a) Color intensity variation for bare car along the line- A; (b) Color intensity variation for bare car along the line- B.

all cases, color intensity of white is plotted along red lines- A (at x/C_L = 0.726) and B (at x/C_L = 0.84) as shown in Figure 15. The zero point of the distance along line lies on top of each Line A and B whereas the bottom point corresponds to the last point on the distance along line axis.

The color intensity graphs for various cases are plotted in this section. The number in horizontal axes indicates the number of pixels covered on the line (along A or B), while vertical axes represents color intensity. In Figure 15 (a), color intensity variation of the bare car along line A shows almost constant values around the center, which indicates separation of flow, where white paint accumulates due to the absence of flow in that region. Whereas along line B, the flow reattaches hence a better variation in color intensity is observed in Figure 15 (b). Figure 16 shows oil-flow visualization for the car with co-rotating VG, whereas Figure 18 shows the same for the car with counter-rotating VG array. A comparison of corresponding color intensity plots (Figures 17 to 19) show high peaks and valleys.

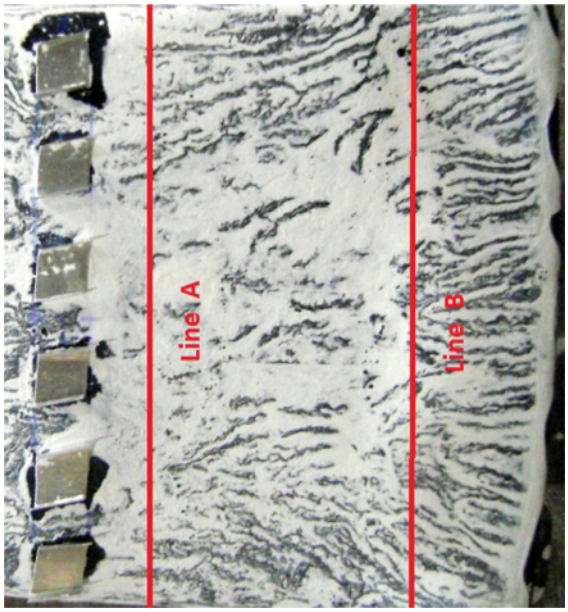

Figure 16. Oil flow visualization at the trunk section of a car with co-rotating VG.

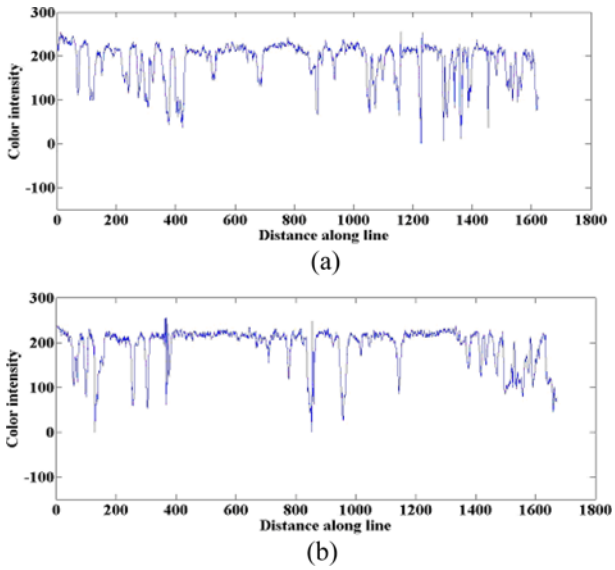

Figure 17. (a) Color intensity variation for car with co-rotating VG array along the line- A; (b) Color intensity variation for car with co-rotating VG array along the line- B.

Figure 19 is indicating effective flow separation achieved using counter-rotating VG.

Smoke flow visualization was carried out as a part of the present study to demonstrate the functional use of rear spoiler, i.e., to impart stability to the car by increasing traction mainly during cross flow condition. Figures 20 (a) and (b) shows smoke flow visualization for the car with and without rear spoiler. As compared to the bare car, the car attached with a rear spoiler exhibits that the flow shifts

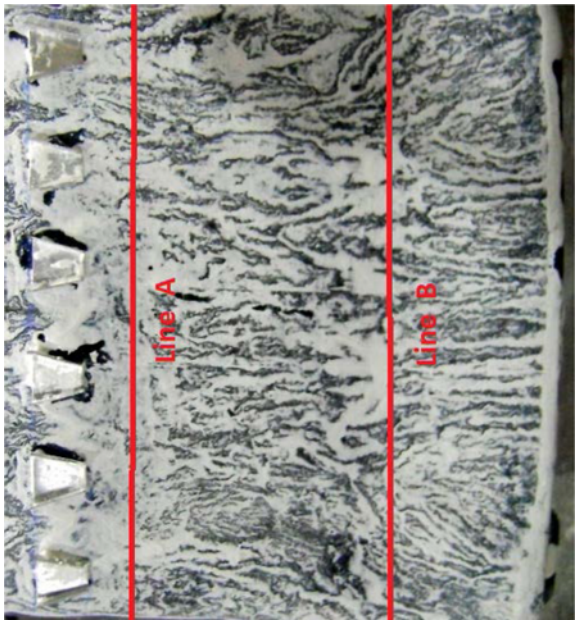

Figure 18. Oil flow visualization at the trunk section of a car with counter-rotating VG.

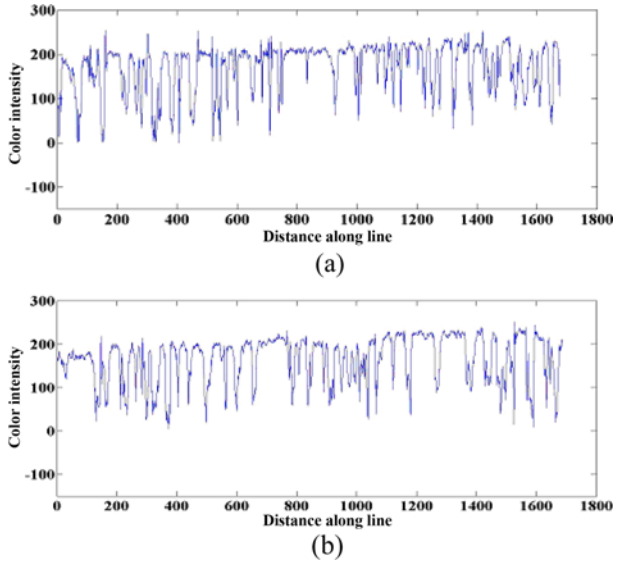

Figure 19. (a) Color intensity variation for car with counter-rotating VG along the line- A; (b) Color intensity variation for car with counter-rotating VG along the line-B.

upwards, indicating a down force acting to the car surface. This down force helps increasing traction between the car tyre and the road maintaining its stability during motion.

4.5. Rear Wake Vortices and Turbulence

The vortex generators (VG) array attached to the roof of the car has an important role to play in both flow separation control and wake vorticity. One might consider it futile to study the wake when already the study of drag has been

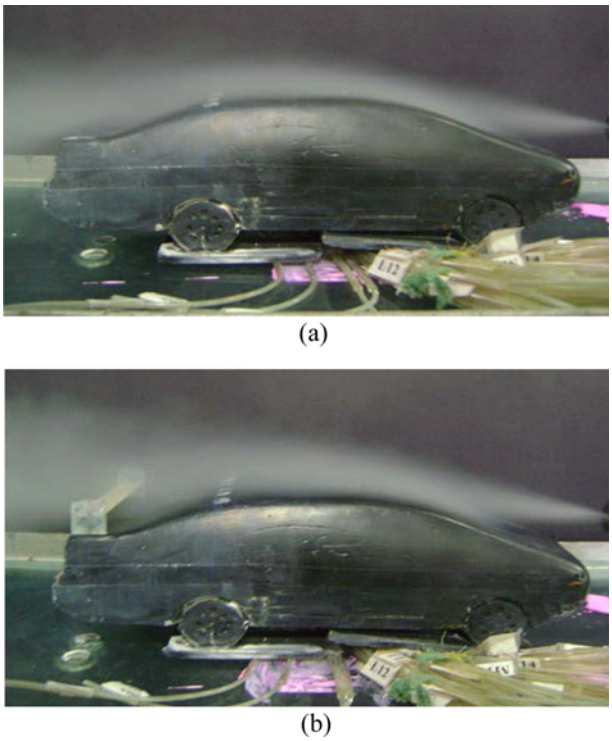

Figure 20. (a) Smoke flow visualization for the car without rear spoiler; (b) Smoke flow visualization for the car with rear spoiler.

thoroughly done with VG array and spoiler. After all, total drag values are reported for various cases that it encompasses the effect of wake. Therefore, it is unnecessary to analyze the wake. However, in this study, wake vortices are analyzed not only in context of drag reduction of the car in discussion, but regarding the effect of wake vortices and wake turbulence on other vehicles behind the car. For high speed car, there is always a threat of wake suction and hence a collision with the vehicle running behind. Adding a device like VG array might add up to the wake turbulence creating a much more hazardous situation. Hence a study of wake vorticity is carried out to

Table 6. Vorticity magnitude and drag coefficient for car at $\beta = 0°$.

Car configuration	Vorticity magnitude	C_D
Bare car facing the wind	394 rad/s	0.3804
Car with counter-rotating VG	266 rad/s	0.2939
Car with co-rotating VG	274 rad/s	0.2942
Car with spoiler ($\alpha = 0°$) and counter-rotating VG	314 rad/s	0.3050
Car with spoiler ($\alpha = +45°$) and counter-rotating VG	348 rad/s	0.3499

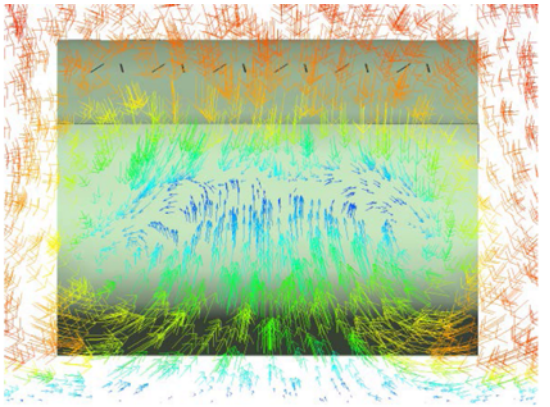

(a)

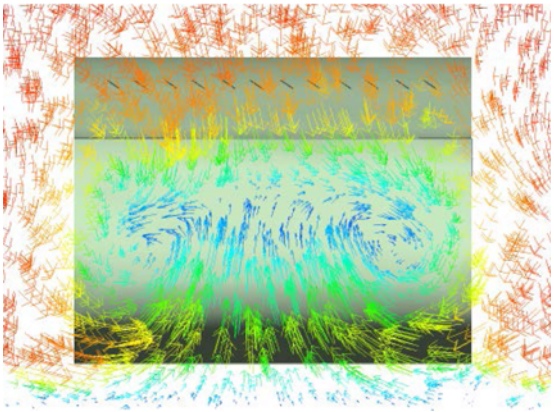

(b)

Figure 21. (a) Velocity vectors showing the rear wake of the car at β = 0° with counter-rotating VG array; (b) Velocity vectors showing the rear wake of the car at β = 0° with co-rotating VG array.

find out the suitable combination of VG array and spoiler, which optimally balances the wake turbulence and the drag. The vorticity is plotted at a plane 20 mm behind the car. Figures 21 (a) and (b) shows the velocity vectors while using co-rotating and counter rotating VG array respectively and the vorticity magnitude are reported in Table 6. Different cases were selected here to be able to correlate the effect of vorticity on the C_D.

Figure 21 supports the values furnished in Table 7, which clearly indicate that the vorticity while using a co-rotating VG array is higher than that for a counter-rotating one. Here vorticity is a manifestation of circulations which in turn is generally accompanied by low pressure regions hence higher vorticity would indicate lower pressures in the wake region making the drag higher.

To evaluate this observation, turbulent kinetic energy (TKE) is plotted in the computational flow domain, with a focus on the wake region along mid-plane of the car length and is shown in Figure 22. Here, line P denotes the front end of the car, line Q shows the point where VG array is placed and line R shows the rear end of the car. The TKE for bare car is higher than that of the cases where VG is

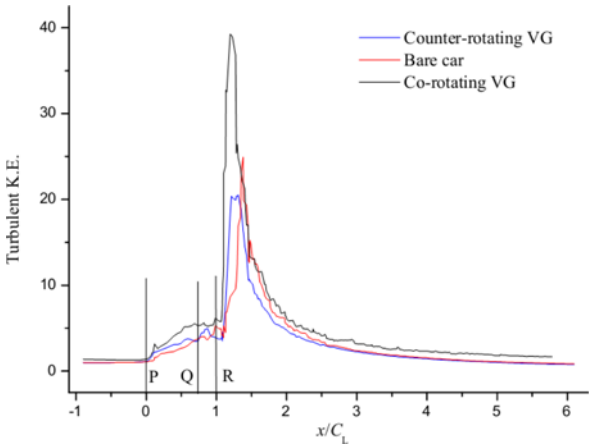

Figure 22. Effects of VG array on turbulent kinetic energy (J/kg) distribution in the computational flow domain.

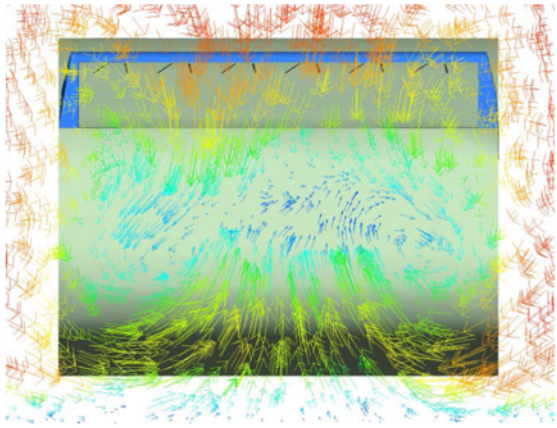

(a)

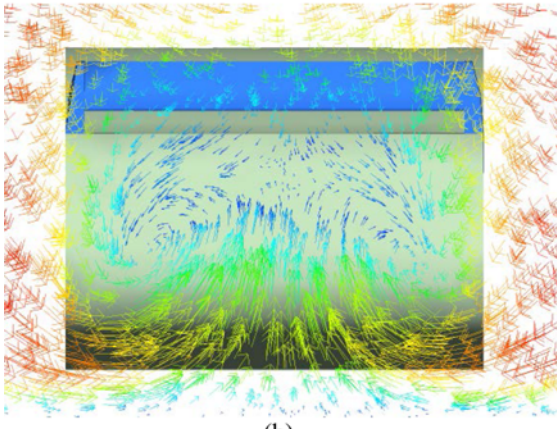

(b)

Figure 23. (a) Velocity vectors showing the rear wake of the car at β = 0° with rear spoiler at a = 0° and counter-rotating VG array; (b) Velocity vectors showing the rear wake of the car at β = 0° with rear spoiler at a = + 45° and counter-rotating VG array.

employed. As the flow separation is delayed with the use of VG array, the wake strength is subsided thus showing a

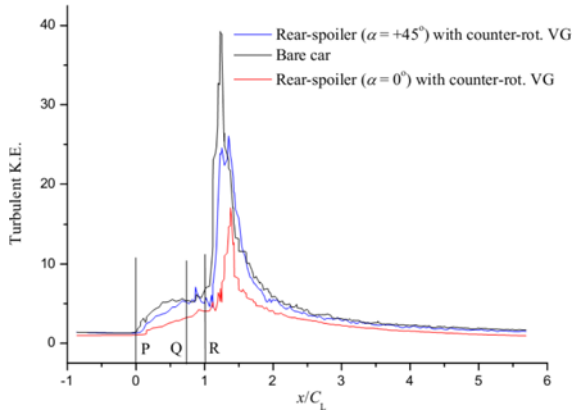

Figure 24. Effects of rear-spoiler and VG array on turbulent kinetic energy (J/kg) distribution in the computational flow domain.

lower value of TKE in the graph. Turbulent kinetic energy as evident from the graph implies that the wake strength in case of counter-rotating VG is less than that with co-rotating VG array.

The comparison shows that the counter-rotating VG array in all aspects is better than the co-rotating one, but even while considering counter-rotating VG array as a better performing flow control device, the effect of rear-spoiler together with the counter-rotating VG array should also be analyzed to observe its effect on the vorticity. Figure 23 shows the wake strength created behind the car for counter rotating VG array with rear-spoiler at a = 0° is lower than that with a = + 45°. The fact is corroborated with the values given in Table 6, which indicate a lower vorticity value for counter-rotating VG with rear-spoiler at a = 0° as compared to the same but at a = + 45°. The fact is further supported by Figure 24, which shows that the peak of the TKE is reduced for counter-rotating VG array with spoiler angle 0° indicating low wake strength behind the car and lower drag, which is evident in Table 6.

It is, therefore, noted that the counter-rotating VG array while used with a rear spoiler at a = 0° reduced drag coefficient considerably (although the lowest value is recorded with counter-rotating VG array alone). But the most important advantage with this combination is the increase in the down force, which restricts the car from skidding. However, the calculation of down force is beyond the scope of this study.

4.6. Calculation on Fuel Saving

This section is included to show the commercial potential of the study albeit using simple arithmetic and simplified reduced model. Heywood (1989) showed that

Fuel consumption (FC) = BSFC × Power.

Therefore, change in fuel consumption can be written as

$$\frac{\Delta FC}{FC} = \eta \times \left(\frac{\Delta C_D}{C_D} + \frac{\Delta S}{S} + \frac{3\Delta U}{U} \right) \quad (4)$$

Whereas, η = property of driving cycle ≈ 0.5 – 0.7 is considered for a passenger car at highway speed,

$\frac{\Delta C_D}{C_D}$ = changes in C_D due to improved aerodynamics,

$\frac{\Delta S}{S}$ = changes due to smaller projected area of the car,

$\frac{3\Delta U}{U}$ = reduction due to highway speed.

The second and third terms of right hand side of Equation (4) are zero in the present case. Therefore,

$$\frac{\Delta FC}{FC} = \eta \times \left(\frac{\Delta C_D}{C_D} \right) \quad (5)$$

Considering maximum reduction in drag coefficient reported in the present study = 0.23,

$\frac{\Delta FC}{FC}$ = 0.5 × .23 = 11.5 %.

Hence, reduction in drag can cut-down the fuel consumption up to 11.5 % for the same velocity, or in other words, one can travel more for a given amount of fuel if VG array is attached to the car. Therefore, vortex generators on passenger car are found beneficial in terms of fuel economy and greenhouse gas reduction.

5. CONCLUSION

Different cases and combinations are analyzed for the car model by varying the air flow angle (β = 0° and ± 30°), spoiler angle (a = 0° and ± 45°) and orientations of vortex generators (co-rotating and counter-rotating) in order to find out the optimum conditions for which drag coefficient is minimum. However, this is pertinent to mention that the wheel movement, roof corner side, and side window angle were not considered in the present study for the sake of simplicity. The following conclusions can be drawn based on the computational analysis of the car model.

(1) Cross flow increases the drag coefficient of the car model.
(2) Higher drag generated by the cross flow can effectively be reduced if both the rear spoiler and VG array are used appropriately.
(3) Car with counter-rotating VG array has minimum value of drag coefficient (C_D = 0.2939) among all the cases studied in this work. The drag coefficient (C_D) is reduced by 23 % as compared to the bare car. This is considered as the most effective case among all. Co-rotating VG array alone can also reduce drag to that extent. However, counter-rotating VG array proves best since it promotes better mixing of flow in its downstream.
(4) Oil flow visualization study also demonstrates the

superiority of counter-rotating VG as a means of flow separation control. Smoke flow visualization supports the functional use of rear spoiler attached to the car.

(5) A number of turbulence models has been tested against the experimental results, and observed that the multi-scale rear wake vortices behind the car model can be effectively captured using the SST k–ω turbulence model and hence it is suitable for the parametric analysis.

(6) The vorticity and turbulence kinetic energy (TKE) analyses indicate that the high vorticity magnitude is responsible for increase the drag and as a result, the TKE is also increased. The counter-rotating VG array while used with a rear spoiler at $a = 0°$ reduced drag coefficient considerably (although the lowest value is recorded with counter-rotating VG alone). But the most important advantage with this combination is the rise in down force, which restricts the car from skidding.

(7) It is calculated that a maximum of 11.5 % fuel consumption can be reduced using best configuration of VG array onto the car surface.

ACKNOWLEDGEMENT–The authors are grateful to the Department of Science and Technology (DST), Government of India for providing financial assistance through DST-FIST grant. The experimental and computational facilities developed with the help of this grant were used in the present study. The authors are also grateful to Shrey Joshi, Aman Jindal, Ajit Verma and Shivam Maurya- the undergraduate students of Motilal Nehru National Institute of Technology Allahabad for experimental data collection and computational modeling.

REFERENCES

Ahmed, S. R. (1981). Wake structure of typical automobile shapes. *J. Fluids Engineering* **103**, **1**, 162–169.

Ahmed, S. R., Ramm, G. and Faltin, G. (1984). Some salient features of the time-averaged ground vehicle wake. *SAE Paper No*. 840300.

Cakir, M. (2012). *CFD Study on Aerodynamic Effects of a Rear Wing/Spoiler on a Passenger Vehicle*. M. S. Thesis. Santa Clara University. Santa Clara, California, USA.

Chan, T. L., Gosse, K., Zhou, Y., Lee, S. C., Wang, X. W. and Huang, J. F. (2008b). Effect of rear slant angle on flow structures and pollutant dispersion in the wake of the studied model vehicle. *Int. J. Heat and Mass Transfer* **51**, **25-26**, 6180–6193.

Chan, T. L., Luo, D. D., Cheung, C. S. and Chan, C. K. (2008a). Large eddy simulation of flow structures and pollutant dispersion in the near-wake region of the studied ground vehicle for different driving conditions. *Atmospheric Environment* **42**, **21**, 5317–5339.

Cheng, S. Y. and Mansor, S. (2017). Rear-roof spoiler effect on the aerodynamic drag performance of a simplified hatchback model. *J. Physics: Conf. Series* **822**, **1**, 1–6.

Cho, J., Kim, T. K., Kim, K. H. and Yee, K. (2017). Comparative investigation on the aerodynamic effects of combined use of underbody drag reduction devices applied to real sedan. *Int. J. Automotive Technology* **18**, **6**, 959–971.

Desai, M., Channiwala, S. A. and Nagarseth, H. J. (2008). Experimental and computational aerodynamic investigations of a car. *WSEAS Trans. Fluid Mechanics* **4**, **3**, 359-368.

Geropp, D. and Odenthal, H. J. (2000). Drag reduction of motor vehicles by active flow control using the Coanda effects. *Experiments in Fluids* **28**, **1**, 74–85.

Gillhaus, A. and Hoffmann, R. (1998). Directional Stability. In: W. Hucho (Ed.) *Aerodynamics of Road Vehicles*. 4th edn. SAE International. Warrendale, Pennsylvania, USA, 239–310.

Guilmineau, E. (2008). Computational study of flow around a simplified car body. *J. Wind Engineering and Industrial Aerodynamics* **96**, **6-7**, 1207–1217.

Hanjalić, K. (1994). Advanced turbulence closure models: A view of current status and future prospects. *Int. J. Heat and Fluid Flow* **15**, **3**, 178–203.

Hassan, S. M. R., Islam, T., Ali, M. and Islam, M. Q. (2014). Numerical study on aerodynamic drag reduction of racing cars. *Procedia Engineering*, **90**, 308–313.

Heft, A. I., Indinger, T. and Adams, N. A. (2012). Introduction of a new realistic generic car model for aerodynamics investigations. *SAE Paper No*. 2012-01-0168.

Heywood, J. B. (1989). *Internal Combustion Engine Fundamentals*. Int. edn. McGraw-Hill. Singapore.

Hucho, W. H. (1998). *Aerodynamics of Road Vehicles*. 4th edn. SAE International. Warrendale, Pennsylvania, USA.

Kang, S. O., Jun, S. O., Park, H. I., Song, K. S., Kee, J. D., Kim, K. H. and Lee, D. H. (2012). Actively translating a rear diffuser device for the aerodynamic drag reduction of passenger car. *Int. J. Automotive Technology* **13**, **4**, 583–592.

Katz, J. (1995). *Race Car Aerodynamics: Designing for Speed*. Bentley Publishers. Cambridge, USA.

Katz, J. (2006). Aerodynamics of race cars. *Annual Review of Fluid Mechanics*, **38**, 27–63.

Kourta, A. and Gilliéron, P. (2009). Impact of the automotive aerodynamic control on the economic issues. *J. Applied Fluid Mechanics* **2**, **2**, 69–75.

Lin, J. C. (2002). Review of research on low-profile vortex generators to control boundary-layer separation. *Progress in Aerospace Sciences* **38**, **4-5**, 389–420.

Menter, F. (1994). Two-equation eddy-viscosity turbulence models for engineering applications. *AIAA Journal* **32**, **8**, 1598–1605.

Rouméas, M., Gilliéron, P. and Kourta, A. (2008). Drag reduction by flow separation control on a car after body. *Int. J. Numerical Methods in Fluids* **60**, **11**, 1222–1240.

Sagar, D. (2010). *Aerodynamic Studies of Rear Spoilers and Vortex Generators on Passenger Car*. M. S. Thesis.

Motilal Nehru National Institute of Technology Allahabad. Prayagraj, India.
Schlichting, H. and Gersten, K. (2007). *Boundary Layer Theory*. 8th edn. Springer-Verlag Berlin Heidelberg. Heidelberg, Germany.
Song, K. S., Kang, S. O., Jun, S. O., Park, H. I., Kee, J. D., Kim, K. H. and Lee, D. H. (2012). Aerodynamic design optimization of rear body shapes of a sedan for drag reduction. *Int. J. Automotive Technology* **13**, **6**, 905−914.
Watkins, S. and Alam, F. (2012). Future vehicle thermal cooling and aerodynamic drag savings: Where will they come from?. *Proc. Int. Conf. Advanced Vehicle Technologies and Integration (VTI2012 SS2006)*, Changchun, China, 75−782.